Enzyme-Capped Relay-Functionalized Mesoporous Carbon Nanoparticles: Effective Bioelectrocatalytic Matrices for Sensing and Biofuel Cell Applications

Alexander Trifonov,[†,§] Katharina Herkendell,[‡,§] Ran Tel-Vered,[†] Omer Yehezkeli,[†] Michael Woerner,[‡] and Itamar Willner[†,*]

[†]Institute of Chemistry, The Center for Nanoscience and Nanotechnology, The Hebrew University of Jerusalem, Jerusalem 91904, Israel, and [‡]Institute of Process Engineering in Life Science, Biomolecular Separation Engineering, Karlsruhe Institute of Technology (KIT), Karlsruhe 76131, Germany. [§]These authors contributed equally to this study.

ABSTRACT The porous high surface area and conducting properties of mesoporous carbon nanoparticles, CNPs (<500 nm diameter of NPs, pore dimensions ~6.3 nm), are implemented to design electrically contacted enzyme electrodes for biosensing and biofuel cell applications. The relay units ferrocene methanol, Fc-MeOH, methylene blue, MB^+, and 2,2′-azinobis(3-ethylbenzothiazoline-6-sulfonic acid), $ABTS^{2-}$, are loaded in the pores of the mesoporous CNPs, and the pores are capped with glucose oxidase, GOx, horseradish peroxidase, HRP, or bilirubin oxidase, BOD, respectively. The resulting relay/enzyme-functionalized CNPs are immobilized on glassy carbon electrodes, and the relays encapsulated in the pores are sufficiently free to electrically contact the different enzymes with the bulk electrode supports. The Fc-MeOH/GOx CNP-functionalized electrode is implemented for the bioelectrocatalyzed sensing of glucose, and the MB^+/HRP-modified CNPs are applied for the electrochemical sensing of H_2O_2. The $ABTS^{2-}$/BOD-modified CNPs provide an effective electrically contacted material for the bioelectrocatalyzed reduction of O_2 (k_{cat} = 94 electrons·s^{-1}). Integration of the Fc-MeOH/GOx CNP electrode and of the electrically wired $ABTS^{2-}$/BOD CNP electrode as anode and cathode, respectively, yields a biofuel cell revealing a power output of ~95 μW·cm^{-2}.

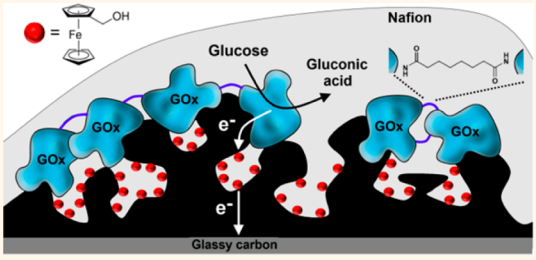

KEYWORDS: mesoporous carbon · electrical wiring · sensor · bilirubin oxidase · oxygen reduction · glucose

The electrical contacting of redox enzymes with electrode supports is a key process in the activation of the bioelectrocatalytic functions of enzymes for amperometric biosensors[1−3] and biofuel cell applications.[4−8] Different methods to electrically contact redox enzymes with electrodes were developed, including the use of diffusional electron transfer mediators,[9,10] tethering of redox relays to the proteins,[11−13] immobilization of the proteins in redox polymer matrices,[14−17] reconstitution of enzymes on relay-cofactor units associated with electrodes,[18] reconstitution of enzymes on cofactor−metal nanoparticle dyads,[19,20] and the electropolymerized integration of enzymes in relay-modified Au nanoparticle matrices.[21] While each of the methods reveals advantages, the different approaches are also accompanied by certain drawbacks and limitations. For example, whereas the reconstitution of apo-enzymes on relay-cofactor units associated with electrodes leads to highly efficient turnover electron transfer, the method is applicable only to monolayer configurations, thus limiting the overall content of the electrically wired enzymes associated with the electrodes. In turn, the immobilization of enzymes in thick redox polymer matrices introduces limitations on substrate transport to the enzyme and difficulties to yield effective charge transfer. Similarly, the direct functionalization of enzymes with redox mediator units leads to their partial deactivation, which is enhanced upon increasing the loading of the

* Address correspondence to willnea@vms.huji.ac.il.

Received for review October 7, 2013 and accepted November 23, 2013.

Published online November 24, 2013
10.1021/nn405218x

mediator, and to a random distribution of relay-modified proteins, which exhibit an average non-optimized loading. Also, the use of diffusional electron transfer mediators often leads to effective electrical contacting of enzymes with electrodes, but such electrodes lack fully integrated electrical wiring features, and interfering cross-talks between the anode and the cathode *via* the diffusional electron mediators often perturb the bioelectrocatalytic functions of the systems.

Carbon-based nanomaterials attract growing interest as functional materials for electrical contacting of redox systems with electrodes.[22−26] The redox features of C_{60} allowed its implementation as an electron mediator for the electrical contacting of redox enzymes with electrodes.[27] Also, the reconstitution of apo-enzymes on cofactor-functionalized carbon nanotubes was applied for the effective electrical communication of redox enzymes with electrodes, and relay-cross-linked carbon nanotubes were applied to activate the bioelectrocatalytic functions of redox proteins.[28] Furthermore, the adsorption of different redox enzymes, such as laccase or bilirubin oxidase, on carbon nanotubes partially unfolded the proteins, thus allowing the electrical communication of their redox centers with the conductive carbon nanotubes and the electrical wiring of the resulting hybrids with macroscopic electrodes.[29−31] Also, the deposition of redox enzymes on graphene, carbon nanotubes, or carbon nanoparticles led to the direct electrical contacting of redox enzymes with electrodes. For example, the deposition of glucose oxidase on graphene led to the bioelectrocatalytic oxidation of glucose.[32,33] Similarly, the adsorption of fructose dehydrogenase or laccase on carbon nanoparticles led to electrically wired enzyme hybrids that stimulated the bioelectrocatalytic oxidation of fructose[34] or the bioelectrocatalyzed reduction of oxygen.[35] Also, redox relay units were tethered to pyrene adsorbed onto carbon nanotubes, and these mediated the electrical wiring of redox enzymes with electrodes.[36]

Mesoporous carbon attracts substantial research interest as a high surface area material exhibiting electrical conductivity. The high surface area features of mesoporous carbon were implemented to remove pollutants[37] or trap materials for controlled delivery.[38,39] Also, the adsorption of redox proteins, such as hemoglobin, on conductive mesoporous carbon was reported to electrically contact redox proteins with macroscopic electrodes.[40]

The different electrically contacted redox enzymes associated with the carbon nanomaterials were extensively studied to design different amperometric sensors or biofuel cell elements.[41−43] In the present study, we introduce the use of mesoporous carbon nanoparticles as a functional material to electrically contact redox proteins with electrodes. Specifically, we discuss the development of "smart" carbon nanoparticles, CNPs, where electron relays are trapped inside the pores by means of redox enzyme caps, resulting in integrated bioelectrocatalytic assemblies. We use the electrically wired enzyme/CNPs for the development of bioelectrocatalytic electrodes acting as sensors or as functional components in biofuel cell elements. We compare the enzyme/CNP-modified electrodes to analogue enzyme/carbon-based material-functionalized electrodes, and we highlight the clear advantages of the enzyme/CNP assemblies over the other systems.

RESULTS AND DISCUSSION

Mesoporous carbon nanoparticles, CNPs (<500 nm diameter, pore dimensions 6.3 nm), were interacted with different redox mediator solutions. The resulting relay-loaded CNPs were deposited and dried on a glassy carbon electrode, followed by the rinsing of the surface with water to remove the excess of non-adsorbed relay molecules. In the following stage, an enzyme, respective to the relay employed, was deposited on the electrode to cap the relay-loaded pores. The resulting protein-modified surfaces were cross-linked by bis(sulfosuccinimidyl) suberate, BS^3, and subsequently, the enzyme-capped relay-loaded mesoporous CNP surface was coated with a 0.5% Nafion solution to yield the integrated bioelectrocatalytic electrode. Using this method, we prepared three relay-loaded mesoporous CNP assemblies, which were capped by three different enzymes. These included (i) ferrocene methanol, Fc-MeOH, -loaded CNPs capped by glucose oxidase, GOx; (ii) methylene blue, MB^+, -loaded CNPs capped by horseradish peroxidase, HRP; and (iii) 2,2′-azinobis(3-ethylbenzothiazoline-6-sulfonic acid), $ABTS^{2-}$, -loaded mesoporous CNPs capped by bilirubin oxidase, BOD. Figure 1 depicts the cyclic voltammograms of the respective enzyme-capped, relay-loaded mesoporous CNP-modified electrodes as a function of scan rates. We find that the peak currents depend linearly on the scan rates, consistent with surface-confined redox species. The entrapment of the relay units in the pores of the CNPs was further supported by Brunauer−Emmett−Teller (BET) analyses. Whereas the unloaded CNPs revealed an average pore dimension of 6.3 nm and surface area of 193 $m^2 \cdot g^{-1}$, with the entrapment of Fc-MeOH, pore dimensions corresponding to 5.5 nm and surface area of 170 $m^2 \cdot g^{-1}$ were revealed. The decrease in the pore dimensions and the nanoparticle surface area is attributed to the partial occupation of the pores by the Fc-MeOH relay. The coulometric analysis associated with the cyclic voltammograms corresponding to the differently capped relay units shown in Figure 1 indicates a loading of 5.0×10^{-8} mol $\cdot g^{-1}$ of CNPs for Fc-MeOH, 1.9×10^{-8} mol $\cdot g^{-1}$ of CNPs for MB^+, and 1.8×10^{-8} mol $\cdot g^{-1}$ of CNPs for $ABTS^{2-}$. Figure S1, Supporting Information, shows the SEM images of the mesoporous CNPs before and after the capping of the pores with GOx. While the

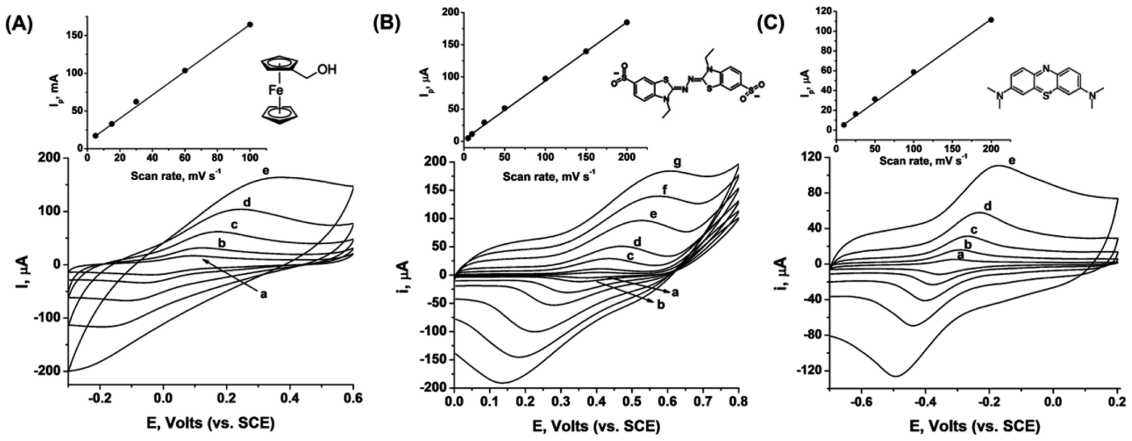

Figure 1. Cyclic voltammograms corresponding to different relay molecules adsorbed on CNP-modified GC electrodes and measured at variable scan rates. (A) Fc-MeOH relay. Scan rates: (a) 5, (b) 15, (c) 30, (d) 60, and (e) 100 mV·s^{-1}. (B) ABTS^{2-} relay. Scan rates: (a) 5, (b) 10, (c) 25, (d) 50, (e) 100, (f) 150, and (g) 200 mV·s^{-1}. (C) MB^{+} relay. Scan rates: (a) 10, (b) 25, (c) 50, (d) 100, and (e) 200 mV·s^{-1}. The insets present the linear dependence observed between the peak oxidation currents and the applied scan rates for the different relay molecules. All measurements were performed in a HEPES buffer (0.1 M, pH = 7.0).

nonmodified particles (Figure S1A) reveal a highly porous structure, the protein-functionalized CNPs show a less porous structure (Figure S1B), consistent with the coverage of the pores by the enzyme. It should be noted that the surface area of the CNPs is *ca.* 25-fold higher than the surface area of graphite (8 m^2·g^{-1}) and *ca.* 3-fold lower in comparison to the surface area of CNTs (520 m^2·g^{-1}). The advantage of the CNPs rests, however, on their porous structure: (i) The pores enable the physical trapping of the relay units through the capping of the pores with the enzymes. In turn, the other carbon materials allow only the physical adsorption and, therefore, the desorption to and from the carbonaceous structures. (ii) The confinement of the relay in the nanosized pores reduces the degrees of freedom for diffusion, and thus, the diffusion rate of the relay toward contacting the redox site of the capping enzyme is increased.

The effect of locking the relay units at the pores of the CNPs by the enzymes was further examined. Figure 2A shows the time-dependent cyclic voltammograms of the Fc-MeOH-loaded CNPs in the absence of the GOx capping, yet protected with the Nafion layer. A rapid depletion of the current is observed, indicating the release of the relay units from the CNPs. In contrast, Figure 2B depicts the time-dependent cyclic voltammograms of the Fc-MeOH relay units capped by GOx and protected by Nafion. The Nafion co-additive assists in adhering and stabilizing the enzyme on the electrode. Evidently, small changes in the currents are observed, implying that the relay is not released from the enzyme-capped CNPs. The initial slight release of Fc-MeOH is attributed to the desorption of the relay molecules from nonpore domains and to Fc-MeOH associated with large pores, which are inefficiently capped by the GOx. It should be noted that after *ca.* 30 min, the amperometric response of Fc-MeOH levels off to a constant value that remains unchanged for several days, implying that the relay units are, indeed, protected in the pores by the enzyme capping units. Figure 2C compares the rates of release of Fc-MeOH from the enzyme-locked and from the enzyme-free Fc-MeOH-loaded CNPs. Evidently, the Fc-MeOH relay units entrapped in the CNP pores by the GOx are effectively protected against leakage from the electrode. This property was observed, also, for the other enzyme-capped, relay-loaded CNP systems (for example, Figure S2 shows the effect of BOD on the locking of ABTS^{2-} at the pores of the CNPs).

The effect of the carbon material on the retention of the relay units in the matrix was further examined by immobilization of the relay molecules on single-walled carbon nanotubes, SWCNTs, and the surface capping of the relay-modified SWCNTs with the respective enzymes and the Nafion film. Figure 3A depicts the time-dependent cyclic voltammograms of Fc-MeOH associated with the SWCNTs/GOx/Nafion assembly. A rapid depletion of the voltammograms is observed, implying that Fc-MeOH is released from the SWCNTs. Similarly, Figure 3B shows the time-dependent cyclic voltammograms of ABTS^{2-} associated with the SWCNTs and protected by BOD and Nafion. A time-dependent decrease in the redox currents associated with the ABTS^{2-} relay is clearly observed, yet the rate of release of ABTS^{2-} from the SWCNTs is smaller compared to that of Fc-MeOH. The slower release of ABTS^{2-} is attributed to the π-stacking of ABTS^{2-} to the SWCNTs. Comparison of the release process of ABTS^{2-} from the BOD/Nafion-capped CNPs (Figure S2C, curve (a)) and the release of ABTS^{2-} from the BOD/Nafion-capped SWCNTs (Figure 3C) indicates, however, that while this relay molecule is fully protected at the CNP matrix, it is being slowly released from the SWCNTs. The release of Fc-MeOH from an analogous graphite assembly was further examined by the adsorption of Fc-MeOH on graphite flakes, followed by the encapsulation of the

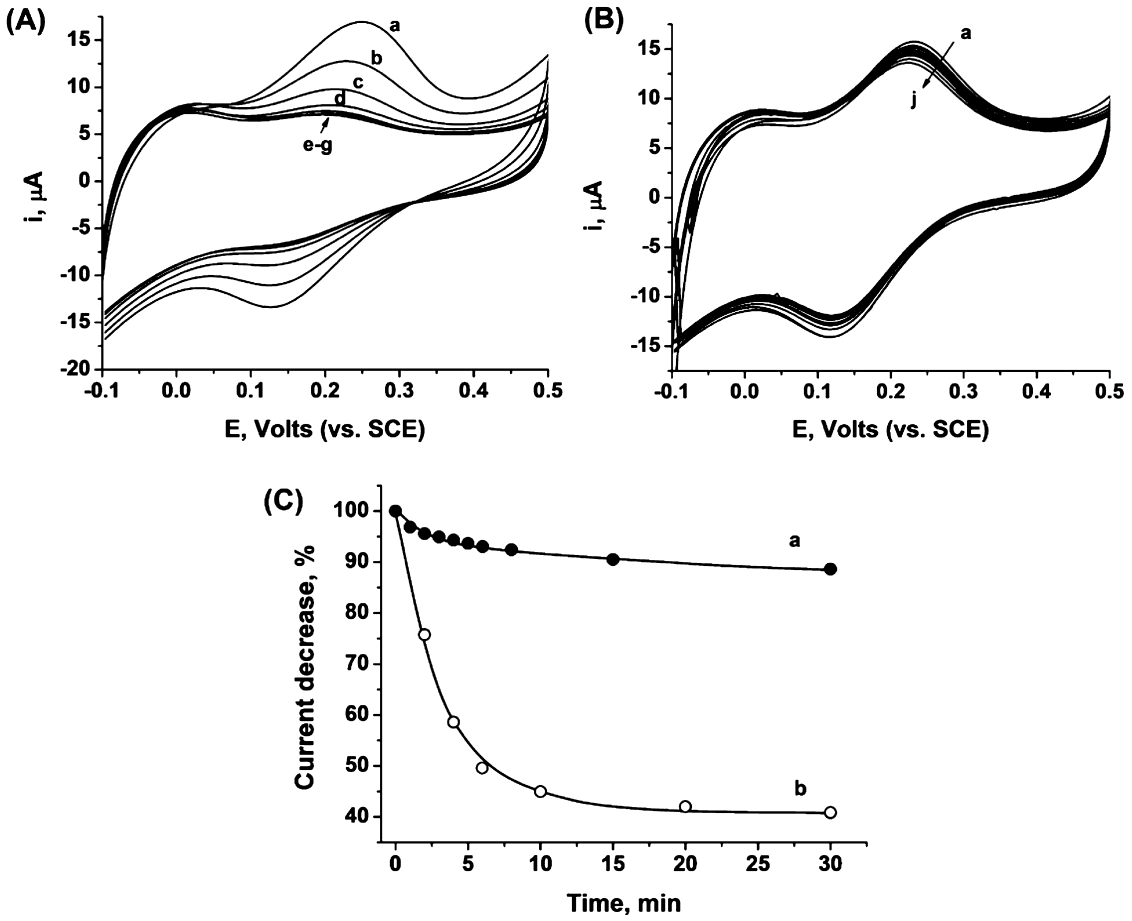

Figure 2. (A) Cyclic voltammograms corresponding to the time-dependent release of Fc-MeOH from Fc-MeOH-loaded CNP-modified electrode, following the immersion of the electrode in HEPES buffer (0.1 M, pH = 7.0) for (a) 0, (b) 2, (c) 4, (d) 6, (e) 10, (f) 20, and (g) 30 min. Scan rate 20 mV·s^{-1}. (B) As in (A), for GOx-capped, Fc-MeOH-loaded CNP-modified electrode. Time intervals of immersion: (a–j) 0–30 min. (C) Time-dependent relative decrease in the amperometric responses by (a) GOx-capped Fc-MeOH-loaded CNP-modified electrode and (b) Fc-MeOH-loaded CNP-modified electrode.

relay in a cross-linked GOx/Nafion layer. Figure 4A depicts the time-dependent cyclic voltammograms of the Fc-MeOH relay associated with the graphite assembly. A rapid decrease in the currents is observed, indicating the release of the relay units from the graphite matrix. Figure 4B compares the time-dependent amperometric responses obtained following the adsorption of Fc-MeOH on the three carbon matrices (mesoporous CNPs, SWCNTs, and graphite). Evidently, the Fc-MeOH associated with the CNPs is protected against release. This is attributed to the encapsulation of the relay in the CNP pores and its capping by the enzyme, a configuration that protects the relay in the CNPs matrix in the form of an integrated structure.

We then examined the bioelectrocatalytic functions of the enzyme-capped, relay-loaded CNP-modified electrodes. In these experiments, we determined the loading of the enzymes in the respective CNP matrices, using appropriate assays. Figure 5A depicts schematically the GOx-capped Fc-MeOH-loaded CNP configuration assembled on a glassy carbon electrode for the relay-mediated bioelectrocatalyzed oxidation of glucose. The surface coverage of GOx on the mesoporous CNPs was estimated to be *ca.* 1.9×10^{-8} mol·g^{-1} of CNPs (Figure S3A, panel I). The activity of the enzyme associated with the electrode corresponded to 82% of the native enzyme activity (Figure S3B, panel I). Figure 5B shows the cyclic voltammograms and the respective calibration curve corresponding to the bioelectrocatalytic oxidation of variable concentrations of glucose by the GOx-capped Fc-MeOH-loaded CNP-modified electrodes. The resulting electrocatalytic anodic currents are observed at the redox potential of the Fc-MeOH electron mediator, implying that the relay communicates the redox centers of the enzymes with the electrodes. Indeed, in a control experiment, where Fc-MeOH was eliminated from the CNPs, yet the pores were capped with GOx, no electrocatalytic currents were observed. Evidently, the electrocatalytic anodic currents were intensified as the concentration of glucose was increased, and a saturation current of *ca.* 150 μA was observed at a glucose concentration of 80 mM. Knowing the loading of GOx on the CNPs and the saturation current, we estimate the turnover rate of electrons between the enzyme and the electrode to be 995 electrons·s^{-1}. The turnover rate corresponding to

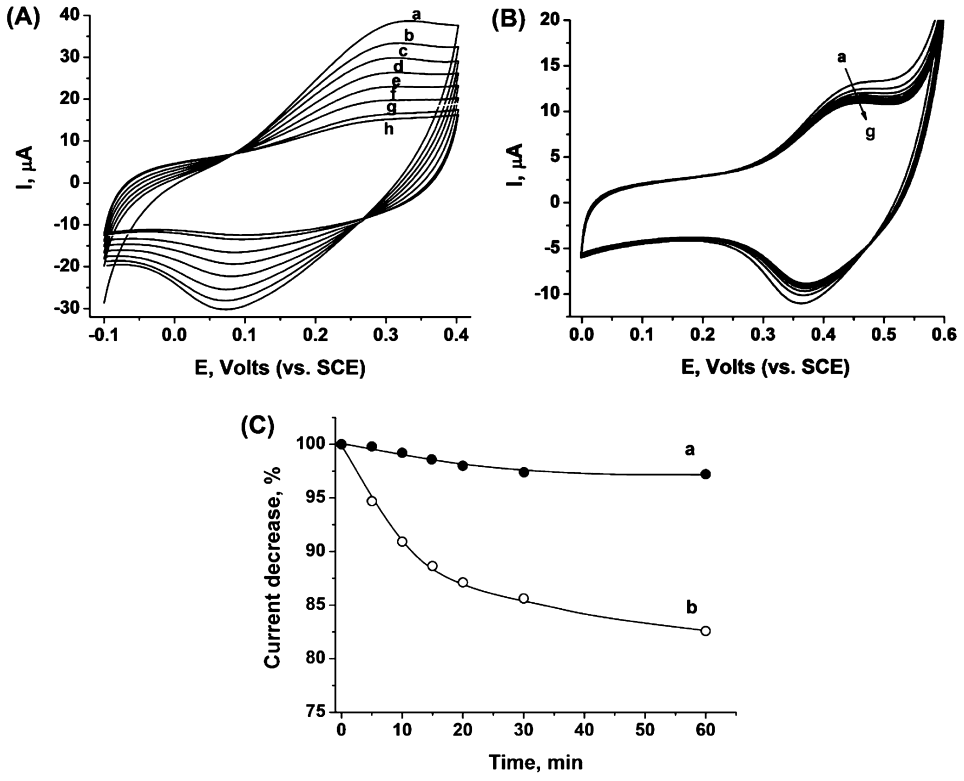

Figure 3. (A) Cyclic voltammograms corresponding to the time-dependent release of Fc-MeOH from Fc-MeOH-loaded GOx-capped SWCNT-modified electrode, following the immersion of the electrode in HEPES buffer (0.1 M, pH = 7.0) for (a) 0, (b) 5, (c) 10, (d) 15, (e) 20, (f) 30, (g) 60, and (h) 90 min. Scan rate 20 mV·s^{-1}. (B) As in (A), for BOD-capped, ABTS^{2-}-loaded SWCNT-modified electrode. Time intervals of immersion: (a−g) 0−60 min. (C) Time-dependent relative decrease in the amperometric responses by (a) BOD-capped, ABTS^{2-}-loaded CNP-modified electrode and (b) BOD-capped ABTS^{2-}-loaded SWCNT-modified electrode.

the bioelectrocatalytic oxidation of glucose by the CNP electrode is by *ca.* 50% higher than the reported rate of electron transfer between the GOx redox center and its native electron acceptor, O_2.[44] This effective electrical communication between the enzyme and the electrode surface suggests that the electrocatalytic currents should be only slightly affected by increasing the levels of oxygen in the electrolyte solution. A comparative analysis testing glucose, 80 mM, on the GOx-capped Fc-MeOH-loaded CNP-modified electrode under air and in O_2-saturated buffer solutions revealed, indeed, only a 10% difference in the electrocatalytic currents (Figure S4). The electrode was then implemented to detect glucose in the concentration range relevant to diabetes. Figure 5C shows the glucose-dependent chronoamperometric responses of the electrode at 0.4 V *vs* SCE and the resulting calibration curve (inset). One may realize that in this concentration range a linear relation between the glucose concentration and the electrocatalytic current exists, suggesting that such electrodes could be implemented for glucose analysis using a single-point calibration process.

A further electrically wired electrode for the bioelectrocatalytic reduction of H_2O_2 involved the horseradish peroxidase (HRP)-capped methylene blue, MB^+-loaded mesoporous CNPs. The loading of HRP on the CNPs was spectroscopically assayed to be *ca.* 1.7 × 10^{-8} mol·g^{-1} of CNPs (cf. Supporting Information). Figure 6 shows the cyclic voltammograms corresponding to the bioelectrocatalyzed reduction of H_2O_2. Control experiments revealed that, in the absence of MB^+, no electrocatalyzed reduction of H_2O_2 occurred, indicating that the MB^+ indeed electrically wired the enzyme with the electrode. As the concentration of H_2O_2 was increased, the electrocatalytic cathodic currents intensified. Figure 6, inset, shows the resulting calibration curve, indicating that, at a H_2O_2 concentration that corresponds to 25 mM, the cathodic currents reach a saturation value of *ca.* 220 μA. Knowing the loading of HRP on the CNPs matrix, we estimated the maximum turnover rate of electrons from the electrode to HRP to be approximately k_{cat} = 1360 electrons·s^{-1}.

A further bioelectrocatalytic electrode based on mesoporous CNPs, which was examined included bilirubin oxidase (BOD) electrically wired through $ABTS^{2-}$-loaded CNPs. Bilirubin oxidase was previously directly wired to electrodes by the partial unfolding of the enzyme units on carbon nanotubes.[45,46] Furthermore, it was established that 2,2′-azinobis(3-ethylbenzothiazoline-6-sulfonic acid), $ABTS^{2-}$, acts as a mediator for the diffusional wiring of BOD with electrode surfaces. In view of this previous art, we addressed the basic questions: (i) Do the mesoporous CNPs exhibit

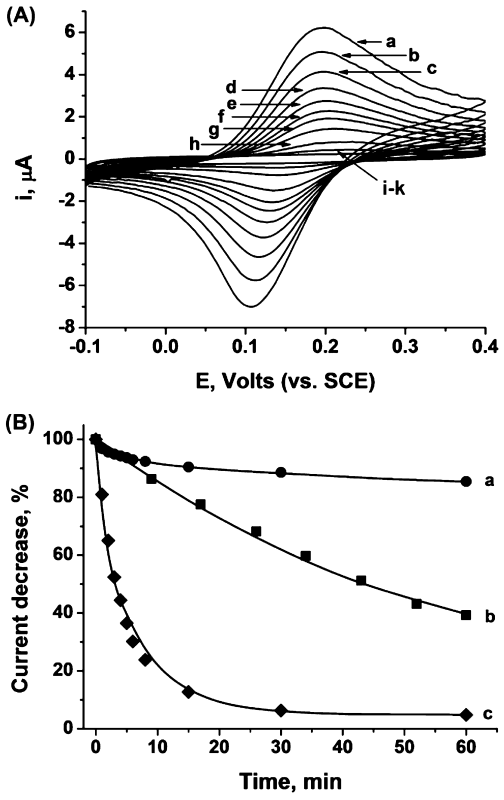

Figure 4. (A) Cyclic voltammograms corresponding to the time-dependent release of Fc-MeOH from GOx-capped, Fc-MeOH-loaded graphite-modified electrode, following immersion in HEPES buffer (0.1 M, pH = 7.0) for (a) 0, (b) 1, (c) 2, (d) 3, (e) 4, (f) 5, (g) 6, (h) 8, (i) 15, (j) 30, and (k) 60 min. Scan rate 20 mV·s^{-1}. (B) Time-dependent relative decrease in the amperometric responses by the GOx-capped: (a) Fc-MeOH-loaded CNPs-modified electrode, (b) Fc-MeOH-loaded SWCNTs-modified electrode, and (c) Fc-MeOH-loaded graphite-modified electrode.

similar properties to SWCNTs, reflected by the adsorption of BOD onto the carbon material and the direct electrical wiring of BOD with the electrode *via* partial unfolding of the enzyme? (ii) Does the entrapment of $ABTS^{2-}$ in the pores of the CNPs improve the electrical contacting of BOD with the electrode? And is the bioelectrocatalytic reduction of O_2 by the $ABTS^{2-}$-loaded CNPs significantly improved as compared to the BOD/SWCNT system?

Figure 7A shows the cyclic voltammograms corresponding to the BOD-capped $ABTS^{2-}$-loaded CNPs. Under N_2, the quasi-reversible redox wave of $ABTS^{2-}$ is detected, curve (a), implying that, indeed, the pores are loaded with $ABTS^{2-}$. Under air, curve (b), as well as under O_2, curve (c), electrical cathodic currents are observed. The cathodic current observed under O_2 is intense and indicates an effective reduction of O_2 to H_2O, at $E = +0.45$ V *vs* SCE. We then analyzed systematically the BOD-catalyzed reduction of O_2 by the CNPs system, in comparison to the SWCNTs system. Figure 7B shows the cyclic voltammograms corresponding to BOD adsorbed and cross-linked on SWCNTs, or on CNPs, and protected by the Nafion film in the absence of the relay molecules. In these experiments, the content of carbon material is identical in the two systems and the coverage of the biocatalyst, BOD, is similar ($1.8 \pm 0.2 \times 10^{-8}$ mol·g^{-1} of carbon). One may realize that both matrices reveal very similar biocatalytic properties toward the reduction of O_2. While under N_2 no electrocatalytic currents are observed, both of the carbon materials electrocatalyze the reduction of O_2. These results suggest that the BOD adsorbed on the CNPs is partially unfolded, similarly to the BOD bound to SWCNTs, a process that yields direct electrical contact between the enzyme and the carbon matrices. Figure 7C reveals, however, that the incorporation of $ABTS^{2-}$ to the SWCNT or CNP matrices leads to substantially different bioelectrocatalytic properties toward the reduction of O_2. In these experiments, $ABTS^{2-}$ was adsorbed on the SWCNTs or trapped in the pores of the CNPs, and the carbon material was capped with BOD, followed by cross-linking of the enzyme and its protection by a Nafion film. In both systems, the content of the carbon material was identical, and the coverage of BOD was similar. Under N_2, both carbon matrices revealed the quasi-reversible cyclic voltammogram of $ABTS^{2-}$, indicating the similar coverage of the relay unit on the two carbon matrices. The cyclic voltammograms corresponding to the BOD-electrocatalyzed reduction of O_2 in the presence of $ABTS^{2-}$ on SWCNTs showed, however, an electrocatalytic current, curve (b), only slightly larger compared to the system in the absence of $ABTS^{2-}$. This result implies that $ABTS^{2-}$ has only little effect on the bioelectrocatalyzed reduction of O_2 by the BOD/SWCNT system. In turn, the BOD-capped $ABTS^{2-}$-loaded CNP matrix reveals, at $E = 0.35$ V *vs* SCE, *ca.* 3-fold higher electrocatalytic current, as compared to the $ABTS^{2-}$/BOD/SWCNT system, curve (b′) (this catalytic current is also *ca.* 2-fold higher as compared to the BOD/CNP system lacking the $ABTS^{2-}$). These results indicate that $ABTS^{2-}$, indeed, wires the BOD capping units with the electrode, thus leading to the enhanced electrocatalyzed reduction of O_2. Furthermore, it should be noted that the $ABTS^{2-}$/BOD-capped SWCNT system is unstable, and $ABTS^{2-}$ is desorbed from the SWCNT matrix (the results in Figure 7C, curves (a) and (b), were recorded immediately after the construction of the electrode, under conditions where $ABTS^{2-}$ was still fully adsorbed on the SWCNTs matrix). In contrast, the BOD-capped $ABTS^{2-}$-loaded CNPs revealed prolonged bioelectrocatalytic stability. The $ABTS^{2-}$ was locked in the pores, and the bioelectrocatalytic functions of the BOD decreased by <10% after 2 days. Knowing the maximum cathodic current, which is extracted under saturation of the electrolyte with oxygen, and knowing the surface coverage of BOD, the turnover rate of the enzyme was estimated to be $k_{cat} = 94$ electrons·s^{-1}. It should be noted that for all of the enzyme-protected, relay-encapsulated mesoporous CNP systems, effective electron

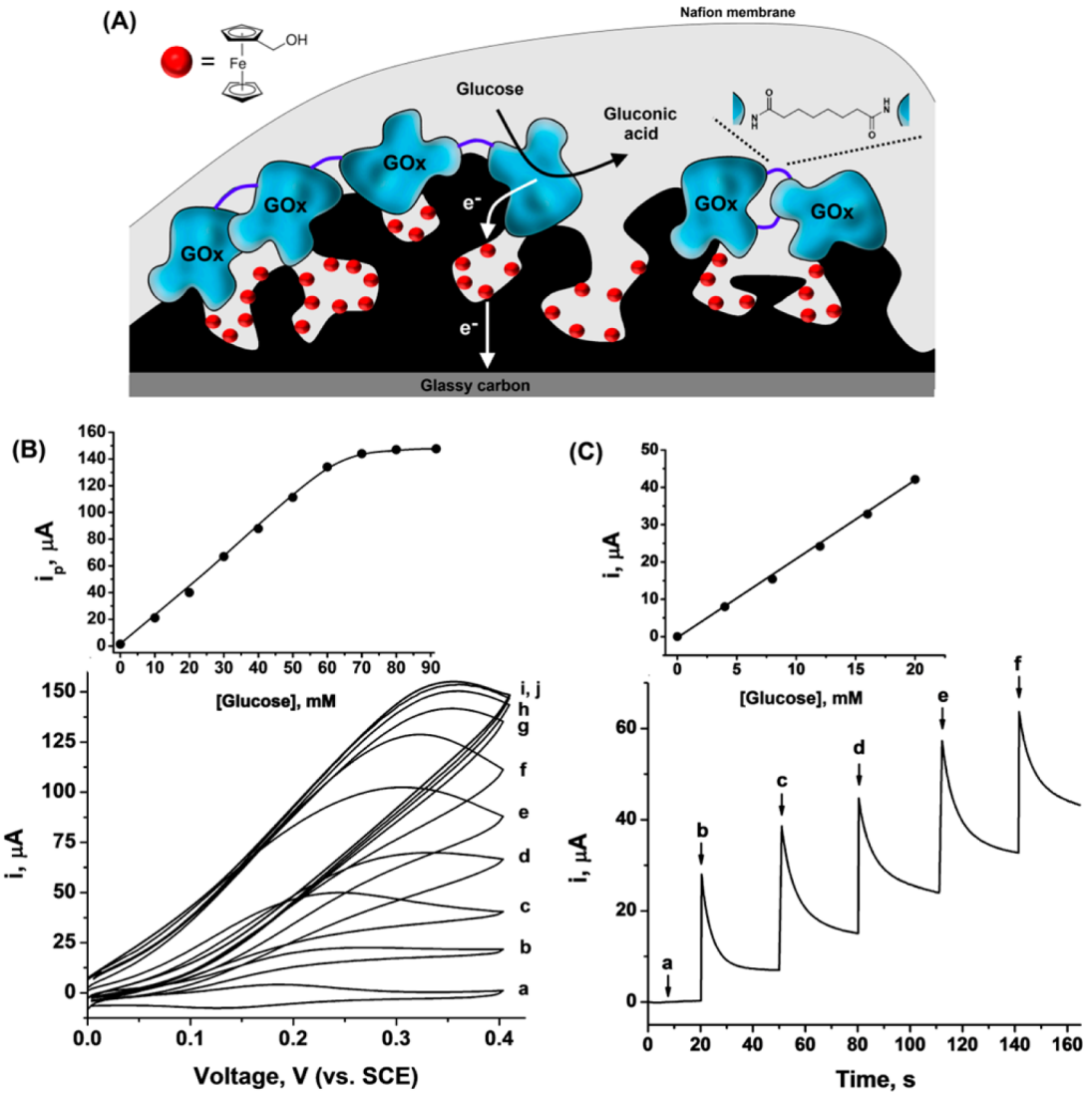

Figure 5. (A) Schematic illustration of the bioelectrocatalytic oxidation of glucose on the GOx-capped, Fc-MeOH-loaded CNP-modified electrode. (B) Cyclic voltammograms corresponding to the bioelectrocatalytic oxidation of variable concentrations of glucose on the GOx-capped, Fc-MeOH-loaded CNP-modified electrode: (a) 0, (b) 10, (c) 20, (d) 30, (e) 40, (f) 50, (g) 60, (h) 70, (i) 80, and (j) 90 mM glucose. Inset: calibration curve corresponding to the amperometric responses at $E = 0.4$ V *vs* SCE for the different concentrations of glucose. Scan rate 5 mV·s^{-1}. (C) Chronoamperometric responses at $E = 0.4$ V for the oxidation of variable concentrations of glucose, relevant to diabetes, on the GOx-capped, Fc-MeOH-loaded CNP-modified electrode: (a) 0, (b) 4, (c) 8, (d) 12, (e) 16, and (f) 20 mM glucose. Inset: calibration curve corresponding to the amperometric responses for the different concentrations of glucose. All measurements were performed in a HEPES buffer (0.1 M, pH = 7.0) under air.

transfer turnover rates for the respective bioelectrocatalytic transformations are observed. Nevertheless, the cyclic voltammograms of the relay-loaded mesoporous CNPs reveal quite a large peak-to-peak separation, implying a nondiffusional electron transfer to the relay units. Indeed, the electron transfer rates between the conductive CNPs and the relays were determined by the Laviron method[47] to be 10, 18, and 13 electrons·s^{-1} for the FcMeOH, MB^+, and $ABTS^{2-}$ relays, respectively. To account for this apparent discrepancy, we note that the electron transfer between the conductive CNPs and the relays is, indeed, nondiffusional, but the confined volume of the nanopores and diminished directional mobility of the relay units in the nanoenvironment increase the diffusion rate of the relay to the capping enzyme units, thereby increasing the probability to electrically contact the enzyme cap with the conductive matrix.

The successful design of the electrically wired GOx-capped Fc-MeOH-loaded CNP anode for the oxidation of glucose and the preparation of the effective BOD-capped $ABTS^{2-}$-loaded CNPs as an electrically wired O_2 reduction cathode paved the way to construct a glucose/O_2 biofuel cell (Figure 8A). The electrocatalytic oxidation of glucose by the Fc-MeOH-mediated process proceeds at an onset potential of $E = -0.05$ V *vs* SCE. In turn, the $ABTS^{2-}$-mediated reduction of O_2 at the BOD-functionalized electrode proceeds at *ca.* $E = +0.45$ V *vs* SCE. This provides a potential difference between the anode and the cathode of *ca.* 0.5 V that

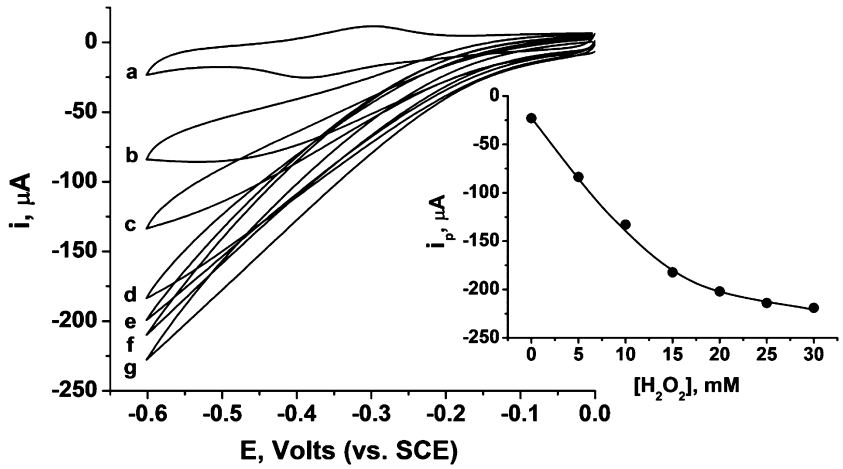

Figure 6. Cyclic voltammograms corresponding to the bioelectrocatalytic reduction of variable concentrations of H_2O_2 on the HRP-capped, MB^+-loaded CNP-modified electrode: (a) 0, (b) 5, (c) 10, (d) 15, (e) 20, (f) 25, and (g) 30 mM H_2O_2. Scan rate 5 $mV \cdot s^{-1}$. Inset: calibration curve corresponding to the amperometric responses at $E = -0.6$ V *vs* SCE for the different concentrations of H_2O_2. Measurements were performed in a HEPES buffer (0.1 M, pH = 7.0) that was purged for 20 min with N_2.

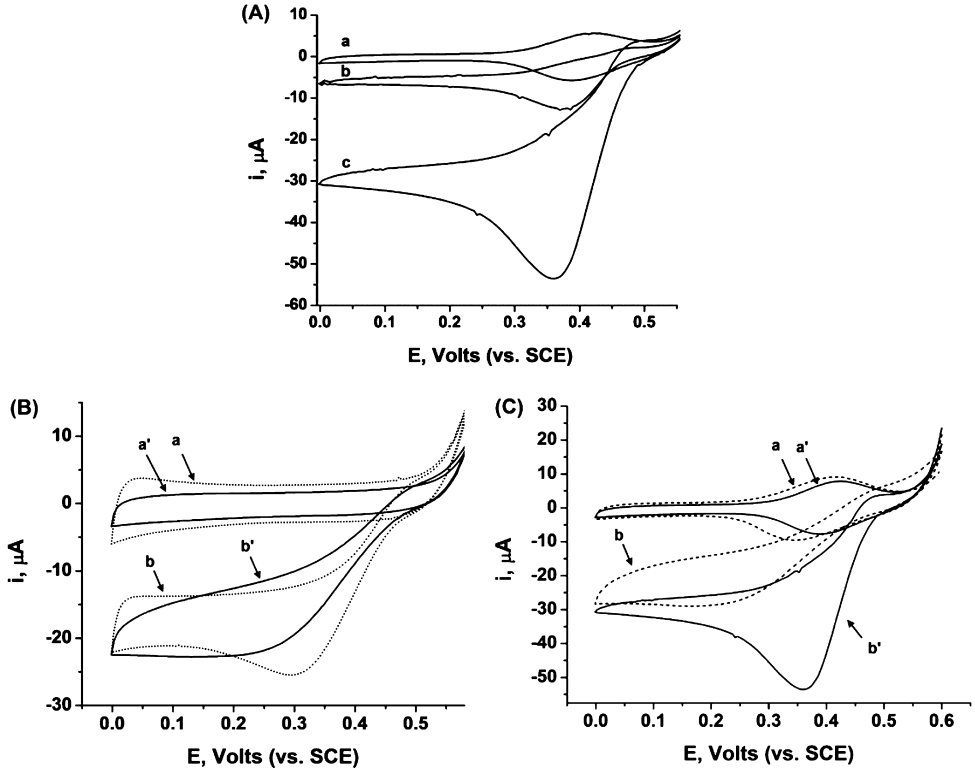

Figure 7. (A) Cyclic voltammograms corresponding to the bioelectrocatalytic reduction of variable concentrations of O_2 on the BOD-capped, $ABTS^{2-}$-loaded CNP-modified electrode: (a) Electrolyte purged with N_2 (b) under air and (c) electrolyte purged with O_2. (B) Cyclic voltammograms corresponding to the bioelectrocatalytic reduction of O_2 on (a) BOD-capped SWCNT-modified electrode in a N_2-purged electrolyte; (b) BOD-capped SWCNT-modified electrode in an O_2-purged electrolyte; (a′) BOD-capped CNP-modified electrode in a N_2-purged electrolyte; (b′) BOD-capped CNP-modified electrode in an O_2-purged electrolyte. (C) Cyclic voltammograms corresponding to the bioelectrocatalytic reduction of O_2 on (a) BOD-capped, $ABTS^{2-}$-loaded SWCNT-modified electrode in a N_2-purged electrolyte; (b) BOD-capped, $ABTS^{2-}$-loaded SWCNT-modified electrode in an O_2-purged electrolyte; (a′) BOD-capped, $ABTS^{2-}$-loaded CNP-modified electrode in a N_2-purged electrolyte; (b′) BOD-capped, $ABTS^{2-}$-loaded CNP-modified electrode in an O_2-purged electrolyte. The HEPES buffer electrolyte (0.1 M, pH = 7.0) was purged for 20 min with either N_2 or O_2. In all measurements, the scan rate was 5 $mV \cdot s^{-1}$.

allows the operation of the biofuel cell. Figure 8B, panel I, shows the discharge (polarization) curve of the biofuel cell, measured at variable external resistances under O_2. The power output of the cell is presented in Figure 8B, panel II, indicating a maximal power of *ca.* $P = 95$ $\mu W \cdot cm^{-2}$. By increasing the potential difference between the electrodes, particularly by implementing relays exhibiting more negative potentials

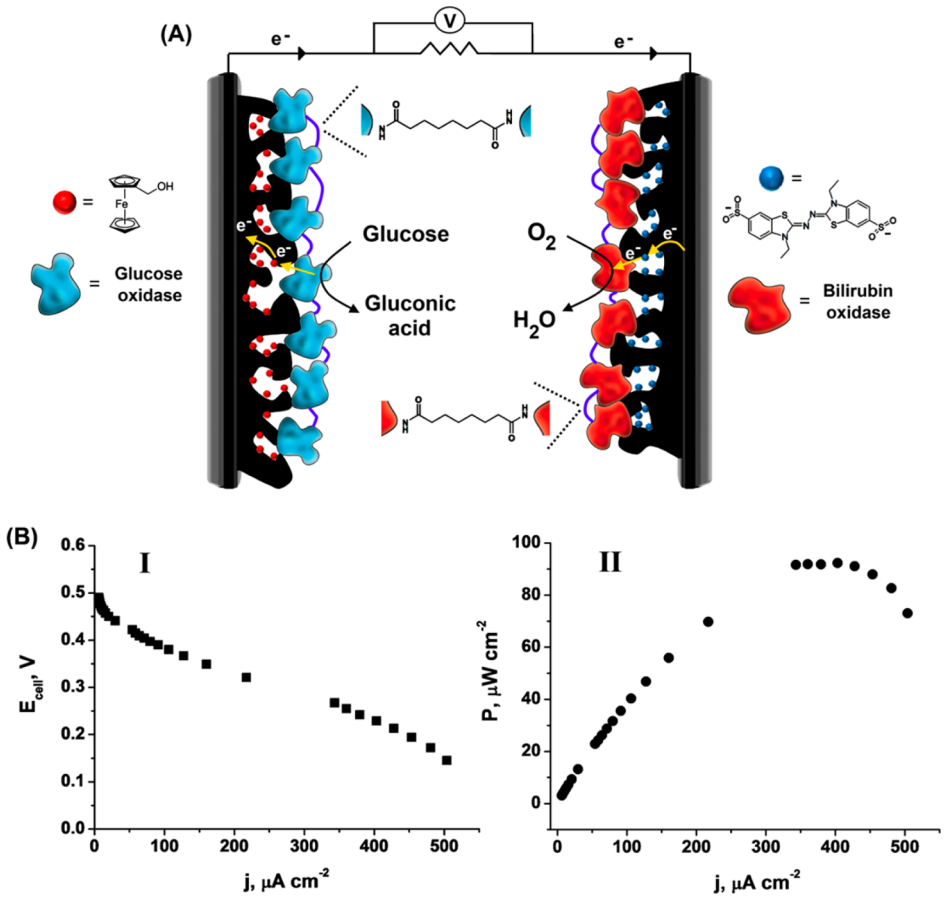

Figure 8. (A) Schematic illustration of the GOx-capped, Fc-MeOH-loaded CNPs//BOD-capped, $ABTS^{2-}$-loaded CNPs biofuel cell. (B) Discharge characteristics of the biofuel cell in (A). Panel I: polarization curve. Panel II: power output. Measurements were performed in a HEPES buffer solution (0.1 M, pH = 7.0) purged for 20 min with O_2 and using variable external resistances.

for the oxidation of glucose, the power output of the cell could be further improved.

CONCLUSIONS

In conclusion, the present study has introduced a new concept to electrically wire redox enzymes and electrodes using mesoporous CNPs. The method is based on the entrapment of relay units in the pores of the CNPs, while capping the pores with the respective redox enzymes. The confinement of the relay units to the conductive mesoporous CNP channels allows the oxidation/reduction of the relays by the conductive matrix and their "interchannel" diffusion to mediate and electrically contact the capping redox enzymes, while retaining the relay units in the pores. The high surface area of the matrices, the close proximity between the relay units and enzymes, and the integrativity of the components (while retaining elements of diffusional electron wiring) represent the advantages of the method.

The present study has applied the method for the electrocatalytic wiring of three enzymes, GOx, HRP, and BOD, and bioelectrocatalytic electrodes for the oxidation of glucose as well as for the reduction of H_2O_2 and O_2, respectively, were prepared. The electrical wiring of other enzymes and the use of other relay systems by this method could be, however, envisaged. Particularly interesting is the development of a new, effective, BOD-based O_2 reduction cathode. This electrically contacted O_2 reduction electrode could be implemented to design biofuel cells of enhanced power outputs as well as photo-bioelectrochemical cells.[48]

MATERIALS AND METHODS

Chemicals. Ferrocene methanol, 2,2′-azinobis(3-ethylbenzothiazoline-6-sulfonic acid) ($ABTS^{2-}$), methylene blue, *N*-methyl-2-pyrrolidone (NMP), Nafion perfluorinated ion-exchange powder solution, mesoporous carbon nanoparticles (CNPs, $d < 500$ nm), single-walled carbon nanotubes, graphite flakes, glucose oxidase, GOx (from *Aspergillus niger*), horseradish peroxidase, HRP (from horseradish), and bilirubin oxidase, BOD (from *Myrothecium verrucaria*), were purchased from Sigma. Polyvinylidene fluoride (PVDF) was purchased from Arkema Innovate Chemistry Company.

A CNP slurry was prepared by mixing 5 mg of CNPs in 0.5 mL of NMP in the presence of 10 μL of either 0.1 M MB^+ (dissolved in water), 0.1 M Fc-MeOH (dissolved in water/ethanol, 1:1 v/v), or 0.1 M $ABTS^{2-}$ (dissolved in water). After 10 min of sonication,

20 μL of a solution containing 10% (w/w) of PVDF in NMP was added, and the resulting suspension was stirred for an additional 20 min. Graphite flakes were sonicated for 1 h prior to their use. SWCNTs and graphite suspensions were similarly prepared.

The fluorophore-functionalized enzymes GOx, HRP, and BOD were prepared by reacting a 1 mL of phosphate buffer solution (0.1 M, pH = 7.2) containing 1 mg of the respective enzyme with 250 μL of dimethyl sulfoxide containing 2 mg·mL^{-1} of the fluorophore Atto-590 NHS (from Fluka). Following 40 min of reaction, the resulting Atto-590-modified enzyme was purified by using a Econo-Pac 10DG column.

Modification of the Electrodes. Glassy carbon (GC) electrodes (d = 3 mm, from ALS Company) were successively polished with 1 and 0.3 μm alumina powder and were further sonicated in water and ethanol for 15 min. Four microliters of the carbon suspension was then deposited on the clean GC surface and was allowed to dry at room temperature. After the rinsing of the electrode in water, 5 μL of 0.3 mg·mL^{-1} enzyme solution (in a 0.1 M HEPES buffer, pH = 7.0) was deposited on the surface and was cross-linked for 15 min using 1 μL of an aqueous solution containing 1 mg·mL^{-1} of bis(sulfosuccinimidyl) suberate, BS^3. The resulting modified electrode was then dried at room temperature, followed by its rinsing with water to remove any remains of nonbound enzyme. The electrodes were then coated with 5 μL of 0.5% Nafion perfluorinated solution and were allowed to dry at room temperature.

Measurements and Instrumentation. Electrochemical measurements were performed using an Autolab potentiostat (ECO Chemie, The Netherlands) driven by a GPES software. A KCl-saturated SCE and a carbon rod (5 mm) were used as the reference and counter electrodes, respectively. UV/visible spectroscopic measurements were performed using a Shimadzu UV-2401 PC spectrophotometer driven by a UVProbe 2.33 software and by employing a quartz cuvette. Emission measurements were performed using a Cary eclipsed fluorescence spectrophotometer (Agilent Technologies) and by employing a quartz cuvette. The biofuel discharge (polarization) curves were recorded under oxygen at variable external resistances and by using an electrometer (Keithley 617). BET measurements were performed using Micrometrics surface area and porosity analyzer, ASAP 2020.

Electron transfer rates, k_{cat}, for the different enzyme electrodes were calculated using the expression $k_{cat} = j/(n \times F \times \Gamma)$, where j is the current density at saturation, n is number of electrons involved in the enzymatic reaction, F is Faraday's constant, and Γ is the surface coverage of the enzyme on the electrode.

Conflict of Interest: The authors declare no competing financial interest.

Acknowledgment. This research is supported by the Nano-SensoMach ERC Advanced Grant No. 267574 under the EC FP7/2007-2013 program. The study was performed under the auspices of the MINERVA Center for Biohybrid Complex Systems. K.H. acknowledges the financial support of the Ernest-Solvay-Stiftung scholarship.

Supporting Information Available: Time-dependent release of $ABTS^{2-}$ from BOD-capped, or noncapped, $ABTS^{2-}$-loaded CNP-modified electrodes, determination of the surface coverage and relative activities of the different enzymes (GOx, HRP, and BOD) attached on the electrodes, and a comparison between the bioelectrocatalytic oxidation of glucose on the GOx-capped, Fc-MeOH-loaded CNP-modified electrode under air or oxygen. This material is available free of charge *via* the Internet at http://pubs.acs.org.

REFERENCES AND NOTES

1. Willner, I.; Katz, E. Integration of Layered Redox Proteins and Conductive Supports for Bioelectronic Applications. *Angew. Chem., Int. Ed.* **2000**, *39*, 1180–1218.
2. Heller, A. Electrical Wiring of Redox Enzymes. *Acc. Chem. Res.* **1990**, *23*, 128–134.
3. Zayats, M.; Willner, B.; Willner, I. Design of Amperometric Biosensors and Biofuel Cells by the Reconstitution of Electrically Contacted Enzyme Electrodes. *Electroanalysis* **2008**, *20*, 583–601.
4. Heller, A. Miniature Biofuel Cells. *Phys. Chem. Chem. Phys.* **2004**, *6*, 209–216.
5. Barton, S. C.; Gallaway, J.; Atanassov, P. Enzymatic Biofuel Cells for Implantable and Microscale Devices. *Chem. Rev.* **2004**, *104*, 4867–4886.
6. Kano, K.; Ikeda, T. Bioelectrocatalysis, Powerful Means of Connecting Electrochemistry to Biochemistry and Biotechnology. *Electrochemistry* **2003**, *71*, 86–99.
7. Willner, I.; Yan, Y.-M.; Willner, B.; Tel-Vered, R. Integrated Enzyme-Based Biofuel Cells: A Review. *Fuel Cells* **2009**, *9*, 7–24.
8. Topcagic, S.; Minteer, S. D. Development of a Membraneless Ethanol/Oxygen Biofuel Cell. *Electrochim. Acta* **2006**, *51*, 2168–2172.
9. Bartlett, P. N.; Tebbutt, P.; Whitaker, R. G. Kinetic Aspects of the Use of Modified Electrodes and Mediators in Bioelectrochemistry. *Prog. React. Kinet.* **1991**, *16*, 55–155.
10. Janda, P.; Weber, J. Quinone-Mediated Glucose Oxidase Electrode with the Enzyme Immobilized in Polypyrrole. *J. Electroanal. Chem.* **1991**, *300*, 119–127.
11. Schuhmann, W.; Ohara, T. J.; Schmidt, H.-L.; Heller, A. Electron Transfer between Glucose Oxidase and Electrodes *via* Redox Mediators Bound with Flexible Chains to the Enzyme Surface. *J. Am. Chem. Soc.* **1991**, *113*, 1394–1397.
12. Degani, Y.; Heller, A. Direct Electrical Communication between Chemically Modified Enzymes and Metal Electrodes. 2. Methods for Bonding Electron-Transfer Relays to Glucose Oxidase and D-Amino-Acid Oxidase. *J. Am. Chem. Soc.* **1988**, *110*, 2615–2620.
13. Willner, I.; Riklin, A.; Shoham, B.; Rivenson, D.; Katz, E. Development of Novel Biosensor Enzyme Electrodes: Glucose Oxidase Multilayer Arrays Immobilized onto Self-Assembled Monolayers on Electrodes. *Adv. Mater.* **1993**, *5*, 912–915.
14. Cosnier, S. Biosensors Based on Immobilization of Biomolecules by Electrogenerated Polymer Films. *Appl. Biochem. Biotechnol.* **2000**, *89*, 127–138.
15. Willner, B.; Katz, E.; Willner, I. Electrical Contacting of Redox Proteins by Nanotechnological Means. *Curr. Opin. Biotechnol.* **2006**, *17*, 589–596.
16. Mao, F.; Mano, N.; Heller, A. Long Tethers Binding Redox Centers to Polymer Backbones Enhance Electron Transport in Enzyme "Wiring" Hydrogels. *J. Am. Chem. Soc.* **2003**, *125*, 4951–4957.
17. Heller, A. Electrical Connection of Enzyme Redox Centers to Electrodes. *J. Phys. Chem. B* **1992**, *96*, 3579–3587.
18. Willner, I.; Heleg-Shabtai, V.; Blonder, R.; Katz, E.; Tao, G.; Bückmann, A. F.; Heller, A. Electrical Wiring of Glucose Oxidase by Reconstitution of FAD-Modified Monolayers Assembled onto Au-Electrodes. *J. Am. Chem. Soc.* **1996**, *118*, 10321–10322.
19. Xiao, Y.; Patolsky, F.; Katz, E.; Hainfeld, J. F.; Willner, I. "Plugging into Enzymes": Nanowiring of Redox Enzymes by a Gold Nanoparticle. *Science* **2003**, *299*, 1877–1881.
20. Zayats, M.; Katz, E.; Baron, R.; Willner, I. Reconstitution of Apo-Glucose Dehydrogenase on Pyrroloquinoline Quinone-Functionalized Au Nanoparticles Yields an Electrically Contacted Biocatalyst. *J. Am. Chem. Soc.* **2005**, *127*, 12400–12406.
21. Yehezkeli, O.; Yan, Y.-M.; Baravik, I.; Tel-Vered, R.; Willner, I. Integrated Oligoaniline-Cross-Linked Composites of Au Nanoparticles/Glucose Oxidase Electrodes: A Generic Paradigm for Electrically Contacted Enzyme Systems. *Chem.—Eur. J.* **2009**, *15*, 2674–2679.
22. Habrioux, A.; Napporn, T.; Servat, K.; Tingry, S.; Kokoh, K. B. Electrochemical Characterization of Adsorbed Bilirubin Oxidase on Vulcan XC 72R for the Biocathode Preparation in a Glucose/O_2 Biofuel Cell. *Electrochim. Acta* **2010**, *55*, 7701–7705.
23. Flexer, V.; Durand, F.; Tsujimura, S.; Mano, N. Efficient Direct Electron Transfer of PQQ-glucose Dehydrogenase

on Carbon Cryogel Electrodes at Neutral pH. *Anal. Chem.* **2011**, *83*, 5721–5727.
24. Katz, E.; Willner, I. Biomolecule-Functionalized Carbon Nanotubes: Applications in Nanobioelectronics. *Chem. Phys. Chem.* **2004**, *5*, 1084–1104.
25. Liu, C.; Alwarappan, S.; Chen, Z.; Kong, X.; Li, C.-Z. Membraneless Enzymatic Biofuel Cells Based on Graphene Nanosheets. *Biosens. Bioelectron.* **2010**, *25*, 1829–1833.
26. Minteer, S. D.; Atanassov, P.; Luckarift, H. R.; Johnson, G. R. New Materials for Biological Fuel Cells. *Mater. Today* **2012**, *15*, 166–173.
27. Patolsky, F.; Tao, G.; Katz, E.; Willner, I. C_{60}-Mediated Bioelectrocatalyzed Oxidation of Glucose with Glucose Oxidase. *J. Electroanal. Chem.* **1998**, *454*, 9–13.
28. Patolsky, F.; Weizmann, Y.; Willner, I. Long-Range Electrical Contacting of Redox Enzymes by SWCNT Connectors. *Angew. Chem., Int. Ed.* **2004**, *43*, 2113–2117.
29. Yan, Y.; Zheng, W.; Su, L.; Mao, L. Carbon-Nanotube-Based Glucose/O_2 Biofuel Cells. *Adv. Mater.* **2006**, *18*, 2639–2643.
30. Gao, F.; Yan, Y.; Su, L.; Wang, L.; Mao, L. An Enzymatic Glucose/O_2 Biofuel Cell: Preparation, Characterization and Performance in Serum. *Electrochem. Commun.* **2007**, *9*, 989–996.
31. Yan, Y.; Yehezkeli, O.; Willner, I. Integrated, Electrically Contacted $NADP^+$-Dependent Enzyme–Carbon Nanotube Electrodes for Biosensors and Biofuel Cell Applications. *Chem.—Eur. J.* **2007**, *13*, 10168–10175.
32. Shan, C.; Yang, H.; Song, J.; Han, D.; Ivaska, A.; Niu, L. Direct Electrochemistry of Glucose Oxidase and Biosensing for Glucose Based on Graphene. *Anal. Chem.* **2009**, *81*, 2378–2382.
33. Kang, X.; Wang, J.; Wu, H.; Aksay, I. A.; Liu, J.; Lin, Y. Glucose Oxidase–Graphene–Chitosan Modified Electrode for Direct Electrochemistry and Glucose Sensing. *Biosens. Bioelectron.* **2009**, *25*, 901–905.
34. Kamitaka, Y.; Tsujimura, S.; Setoyama, N.; Kajino, T.; Kano, K. Fructose/Dioxygen Biofuel Cell Based on Direct Electron Transfer-Type Bioelectrocatalysis. *Phys. Chem. Chem. Phys.* **2007**, *9*, 1793–1801.
35. Szot, K.; Nogala, W.; Niedziolka-Jönsson, J.; Jönsson-Niedziolka, M.; Marken, F.; Rogalski, J.; Nunes Kirchner, C.; Wittstock, G.; Opallo, M. Hydrophilic Carbon Nanoparticle-Laccase Thin Film Electrode for Mediatorless Dioxygen Reduction: SECM Activity Mapping and Application in Zinc-Dioxygen Battery. *Electrochim. Acta* **2009**, *54*, 4620–4625.
36. Ding, S.-N.; Shan, D.; Cosnier, S.; Le Goff, A. Single-Walled Carbon Nanotubes Noncovalently Functionalized by Ruthenium(II) Complex Tagged with Pyrene: Electrochemical and Electrogenerated Chemiluminescence Properties. *Chem.—Eur. J.* **2012**, *18*, 11564–11568.
37. Mauter, M. S.; Elimelech, M. Environmental Applications of Carbon-Based Nanomaterials. *Environ. Sci. Technol.* **2008**, *42*, 5843–5859.
38. Zhu, J.; Liao, L.; Bian, X.; Kong, J.; Yang, P.; Liu, B. pH-Controlled Delivery of Doxorubicin to Cancer Cells, Based on Small Mesoporous Carbon Nanospheres. *Small* **2012**, *8*, 2715–2720.
39. Kim, T.-W.; Chung, P.-W.; Slowing, I. I.; Tsunoda, M.; Yeung, E. S.; Lin, V. S.-Y. Structurally Ordered Mesoporous Carbon Nanoparticles as Transmembrane Delivery Vehicle in Human Cancer Cells. *Nano Lett.* **2008**, *8*, 3724–3727.
40. Ma, G.-X.; Lu, T.-H.; Xia, Y.-Y. Direct Electrochemistry and Bioelectrocatalysis of Hemoglobin Immobilized on Carbon Black. *Bioelectrochemistry* **2007**, *71*, 180–185.
41. Zebda, A.; Gondran, C.; Le Goff, A.; Holzinger, M.; Cinquin, P.; Cosnier, S. Mediatorless High-Power Glucose Biofuel Cells on Compressed Carbon Nanotube–Enzyme Electrodes. *Nat. Commun.* **2011**, *2*, 370.
42. Zhou, M.; Wang, J. Biofuel Cells for Self-Powered Electrochemical Biosensing and Logic Biosensing: A Review. *Electroanalysis* **2012**, *24*, 197–209.
43. Meredith, M. T.; Minteer, S. D. Biofuel Cells: Enhanced Enzymatic Bioelectrocatalysis. *Annu. Rev. Anal. Chem.* **2012**, *5*, 157–179.
44. Bourdillon, C.; Demaille, C.; Gueris, J.; Moiroux, J.; Savéant, J. M. A Fully Active Monolayer Enzyme Electrode Derivatized by Antigen–Antibody Attachment. *J. Am. Chem. Soc.* **1993**, *115*, 12264–12269.
45. Yan, Y. M.; Yehezkeli, O.; Willner, I. Integrated, Electrically Contacted $NAD(P)^+$-Dependent Enzyme-Carbon Nanotube Electrodes for Biosensors and Biofuel Cell Applications. *Chem.—Eur. J.* **2007**, *13*, 10168–10175.
46. Yehezkeli, O.; Tel-Vered, R.; Raichlin, S.; Willner, I. Nano-Engineered Flavin-Dependent Glucose Dehydrogenase/Gold Nanoparticle-Modified Electrodes for Glucose Sensing and Biofuel Cell Applications. *ACS Nano* **2011**, *5*, 2385–2391.
47. Laviron, E. General Expression of the Linear Potential Sweep Voltammogram in the Case of Diffusionless Electrochemical Systems. *J. Electroanal. Chem.* **1979**, *101*, 19–28.
48. Yehezkeli, O.; Tel-Vered, R.; Wasserman, J.; Trifonov, A.; Michaeli, D.; Nechushtai, R.; Willner, I. Integrated Photosystem II-Based Photo-Bioelectrochemical Cells. *Nat. Commun.* **2012**, *3*, 742.